PSU-IRL-SCI-405

Classification Numbers 1.5.3, 3.1.3, and 3.2.2

THE PENNSYLVANIA
STATE UNIVERSITY

IONOSPHERIC RESEARCH

Scientific Report 405

AN EXPERIMENTAL INVESTIGATION OF THE POWER SPECTRUM OF PHASE MODULATION INDUCED ON A SATELLITE RADIO SIGNAL BY THE IONOSPHERE
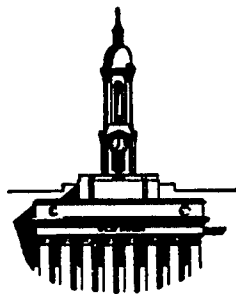
by

David T. Moser

December 12, 1972

IONOSPHERE RESEARCH LABORATORY

University Park, Pennsylvania

DOCUMENT CONTROL DATA - R & D

(Security classification of title, body of abstract and indexing annotation must be entered when the overall report is classified)

1. ORIGINATING ACTIVITY (Corporate author)	2a. REPORT SECURITY CLASSIFICATION
Ionosphere Research Laboratory	2b. GROUP

3. REPORT TITLE

An Experimental Investigation of the Power Spectrum of Phase Modulation Induced on a Satellite Radio Signal by the Ionosphere

4. DESCRIPTIVE NOTES *(Type of report and inclusive dates)*

Scientific Report

5. AUTHOR(S) *(First name, middle initial, last name)*

David T. Moser

6. REPORT DATE	7a. TOTAL NO. OF PAGES	7b. NO. OF REFS
December 12, 1972	64	

8a. CONTRACT OR GRANT NO.	9a. ORIGINATOR'S REPORT NUMBER(S)
NASA NGR 39-009-002 NSF GA-12228	PSU-IRL-SCI-405
b. PROJECT NO.	
c.	9b. OTHER REPORT NO(S) (Any other numbers that may be assigned this report)
d.	

10. DISTRIBUTION STATEMENT

Sponsoring Agencies

11. SUPPLEMENTARY NOTES	12. SPONSORING MILITARY ACTIVITY
	National Aeronautics and Space Administration National Science Foundation

13. ABSTRACT

The object of this study was to investigate the power spectrum of phase modulation imposed upon satellite radio signals by the inhomogeneous F-region of the ionosphere (100 - 500 km). Tapes of the S-66 Beacon B Satellite recorded during the period 1964 - 1966 were processed to yield or record the frequency of modulation induced on the signals by ionospheric dispersion. This modulation is produced from the sweeping across the receiving station (State College, Pennsylvania) as the satellite transits of the two-dimensional spatial phase pattern are produced on the ground. From this a power spectrum of structure sizes comprising the diffracting mechanism was determined using digital techniques. Fresnel oscillations were observed and analyzed along with some comments on the statistical stationarity of the shape of the power spectrum observed.

DD FORM 1473 (PAGE 1)

S/N 0101-807-6811

NONE

A-31408

Scientific Report 405

An Experimental Investigation of the Power Spectrum of Phase Modulation Induced on a Satellite Radio Signal by the Ionosphere
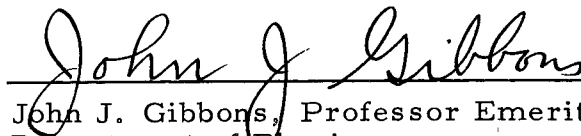
by

David T. Moser

December 12, 1972

Submitted by: _____

W. J. Ross, Head, Department of
Electrical Engineering
Project Supervisor

_____

John J. Gibbons, Professor Emeritus,
Department of Physics

Approved by: _____

A. J. Ferraro, Acting Director
Ionosphere Research Laboratory

Ionosphere Research Laboratory

The Pennsylvania State University

University Park, Pennsylvania 16802

ACKNOWLEDGMENTS

TABLE OF CONTENTS

LIST OF TABLES

LIST OF FIGURES

CHAPTER I

INTRODUCTION

1.1   Previous Related Studies

The ionosphere is the region of the upper atmosphere comprised of neutral and ionized gases and free electrons. The presence of free ions and electrons is caused mainly by photoionization during direct sunlight conditions, and is maintained during nighttime conditions by the finite recombination rates of the ionized particles. Although there are not any definite boundaries given to this region, it is generally considered to start at an altitude of 50 km and continue upward to the interface between the atmosphere and the solar wind.

Active investigation of this region began half a century ago when it was observed (Appleton and Barnett 1925) that radio waves from ground based senders were reflected from an altitude of 100 to 200 km. Using this reflection technique, researchers were able to generate fairly detailed descriptions of the ionosphere. They also found that the ionized medium was not uniform or static, but at times contained random fluctuations in electron density which caused amplitude fluctuations or scintillations of the returned echoes. Further investigations of this effect produced some information on the size and motion of these inhomogeneous structures.

This method contained two fundamental difficulties:

(1) it was limited to analysis of the region below the height of maximum ionization since no reflections could be obtained from greater heights, (2) the mathematical description of this process near the reflection point was complex and obscured the interpretation of the experimental data. A new experimental technique was introduced by Hewish (1951) which eliminated the first problem and reduced the complexity of the second. He introduced the idea of using a radio star with its higher frequencies as the source in a transmission experiment. Further improvement has occurred in the last ten years with the introduction of satellite radio sources. These have the advantage of providing very coherent and stable signals with the ability to scan large sections of the ionosphere very quickly during the transit of the satellite across the field of view of a receiving station.

To date most transmission experiments have dealt with the amplitude variations of the radio signal. Amplitude studies by Spencer (1955) showed the irregularities to be elongated along the magnetic field lines, and studies by Jones (1960) produced a range of apparent sizes of these structures. Further studies (Jespersen et al., 1964; Dyson, 1969; Kelleher et al., 1970; Rufenach et al., 1972) have produced information on the statistical nature of their location, size, and shape.

The experimental use of phase fluctuations rather than amplitude scintillation, has not received much attention except for a study by Porcello and Hughes (1968)

due probably to its much greater experimental complexity.
As will be shown later, however, the use of phase infor-
mation has the advantage of allowing the observation of
larger structure sizes than by amplitude studies for a given
source frequency and allowing a more direct interpretation
of the results in terms of the ionospheric characteristics.

1.2 Statement of the Problem

The object of this study is to investigate the power
spectrum of phase modulation imposed upon satellite radio
signals by the inhomogeneous F-region of the ionosphere
(100-500 km). Records containing the signals will be pro-
cessed to yield temporal variations resulting predominately
from the sweep across a receiving station as the satellite
transits, of the two-dimensional spatial phase pattern
produced on the ground. This will then be linked to the
power spectrum of structure sizes comprising the diffracting
medium. It is hoped that these results may provide useful
information on the nature of the diffracting medium and on
possible production mechanisms for its inhomogeneous nature.

CHAPTER II

THEORY OF DIFFRACTION DUE TO AN INHOMOGENEOUS IONOSPHERE

2.1   Diffraction Theory

It is necessary to develop a physical model and the
associated mathematical description of the transmission
experiment being conducted. The most general model is that
of a moving point source at a finite distance from the
diffracting medium of finite thickness. The motion of the
source will cause the geometry of the problem to change by
changing the angle of incidence upon the medium and the
distances between source and diffracting medium and observer.
The simplified model to be used is of a uniform, unit ampli-
tude plane wave normally incident upon a thin diffracting
medium. Later the restriction to use of a plane wave
(source at infinite distance) will be lifted. Use will be
made of diffraction theory (outlined by Ratcliffe 1956) to
describe the physical model used.

The diffracting medium modifies both the amplitude
A and phase ϕ of the plane wave, so that as it leaves the
medium it possesses a complex amplitude $\bar{f}$ (x,y) across the
plane parallel to the medium (complex quantities are indi-
cated by a bar) given by:

$$\bar{f}(x,y) = A(x,y) \exp[i\phi(x,y)] \qquad 2.1$$

The wave field immediately below the plane of the medium,

4

and hence at all points in this half-space, can be repre-
sented by an angular spectrum of plane waves $\overline{A}$ (θ_1, θ_2)
incident upon the diffracting medium at the angles θ_1, θ_2
(θ_1 is the complement of the angle between the propagation
vector $\hat{k}$ and the x axis, similarly for θ_2 and the y axis).
What this involves is taking the vector sum of the angular
components shifted in phase by an appropriate amount, with
x=y=0 taken as the reference point for zero phase shift.
Letting $C_j = \cos \theta_j$ and $S_j = \sin \theta_j$ for $j = 1,2$, $\overline{A}(\theta_1, \theta_2)$
becomes

$$\overline{A}(\theta_1, \theta_2) = \overline{F}(S_1, S_2)$$

The complex amplitude in terms of its angular spectrum is
(lower case dimensions and coordinates x,y,z are normalized
in terms of wave length λ, upper case letters represent
unnormalized distances)

$$\overline{f}(x,y) = \int_{-1}^{1} \int_{-1}^{1} \overline{F}(S_1, S_2) \exp[2\pi i(S_1 x + S_2 y)] ds_1 \, ds_2$$

$$2.2$$

As the wave front leaves the medium the individual elements
of $\overline{F}(S_1, S_2)$ are shifted in phase by an amount $2\pi C_3 z$. As
used here, the sines of θ_1 and θ_2 along with C_3 form the
direction cosines of $\hat{k}(\theta_1, \theta_2)$. C_3 is related to θ_1 and θ_2
by

$$C_3 = [- \cos(\frac{\pi}{2} - \theta_1 + \frac{\pi}{2} - \theta_2) \cos(\frac{\pi}{2} - \theta_1 - \frac{\pi}{2} + \theta_2)]^{\frac{1}{2}}$$

or

$$C_3 = [\cos(\theta_1 + \theta_2) \cos(\theta_1 - \theta_2)]^{\frac{1}{2}}$$

For a given distance from the screen, equation 2.2 becomes

$$\bar{f}(x,y,z) = \int_{-1}^{1} \int_{-1}^{1} \bar{F}(S_1,S_2) \exp[2\pi i[S_1 x + S_2 y + C_3 z]]ds_1 \, ds_2$$

2.3

When $S > 1$, $(1 - C^2) > 1$ yields imaginary values for C. Letting $C_3 = i\gamma$ for real γ, the term $\exp(2\pi i C_3 z)$ in equation 2.3 becomes $\exp(- 2\pi \gamma z)$. Waves with $S > 1$ are therefore greatly attenuated as they leave the screen and so carry no power away from the screen. They are commonly referred to as evanescent waves. For the consideration of wave fields at a distance of many wavelengths below the medium, the limits of integration in equations 2.2 and 2.3 can be extended to $\pm \infty$ to yield

$$\bar{f}(x,y,z) = \int_{-\infty}^{\infty} \int_{-\infty}^{\infty} \bar{F}(S_1,S_2) \exp[2\pi i(S_1 x + S_2 y + C_3 z)]ds_1 \, ds_2$$

Previously phase was measured w.r.t. the carrier at the diffracting medium. In evaluating the spectrum at a distance z from the screen, only phase measured w.r.t. the carrier at the point of observation will be used. This change is accomplished by subtracting the phase factor $2\pi i z$

from the $2\pi iC_3z$ term above to yield

$$\bar{f}(x,y,z) = \int_{-\infty}^{\infty}\int_{-\infty}^{\infty} \bar{F}(S_1,S_2)\ \exp[2\pi i(S_1x+S_2y+(C_3-1)z)]ds_1\ ds_2$$

$$2.4$$

Comparing equation 2.4 with 2.2, $\bar{f}(x,y,z)$ is composed of a complex angular spectrum

$$\bar{G}(S_1,S_2,z) = \bar{F}(S_1,S_2)\ \exp[2\pi i(C_3-1)z] \qquad 2.5$$

which can be thought of as the function $\bar{F}(S_1,S_2)$ with its components shifted in phase to account for propagation in different directions to a distance z from the screen. As will be shown later, it is $\bar{f}(x,y,z)$ which is actually measured and the angular spectrum is used as a means of determining the nature of the diffracting medium from the measured pattern $\bar{f}(x,y,z)$. Equation 2.4 is the expression for a Fourier transform pair, with z as a parameter, and can be represented as:

$$\bar{f}(x,y,z) \leftrightarrow \bar{G}(S_1,S_2,z) \qquad 2.6$$

If the case of a diffracting medium with no absorption (which is a good approximation for the F-region at the frequencies used) is considered, $\bar{f}(x,y,0)$ will contain only phase variations. This is equivalent to setting $A(x,y) = 1$ in equation 2.1. An attempt will be made to obtain predictions about the properties of the diffraction pattern by

considering a simple diffracting medium with a cosinusoidal variation of phase shift with position. The generalization of this model to more complex medium distributions will be then considered. The inversion of the results of this analysis will provide a basis for interpreting experimentally obtained data.

2.2 Fourier Analysis of a Weakly Refracting Screen

In the interest of simplicity only variations in the x direction will be considered. Let $\bar{f}(x,0)$ consist of a cosinusoidal phase variation imposed on a unit amplitude carrier given by

$$\bar{f}(x,0) = \exp(i\phi_o \cos 2\pi\tfrac{x}{d}) \qquad 2.7$$

where d is the periodicity of the modulation and therefore of the screen. If $\phi_o \ll 1$, then $\bar{f}(x,o) \simeq 1 + i\phi_o \cos 2\pi\tfrac{x}{d}$ which can be shown to have the following angular spectrum (the values of S in the parentheses indicating the angle of the component).

$$\bar{F}(S) = 1 \ (S = 0) + \frac{i\phi_o}{2} \ (S = \tfrac{1}{d}) + \frac{i\phi_o}{2} \ (S = -\tfrac{1}{d})$$

The first term represents the carrier and the other two terms are phase quadrature terms. Letting the integral in equation 2.4 (without the y dependence) become a sum, $\bar{f}(x,z)$ becomes:

$$\bar{f}(x,z) = \sum_j \{[\bar{F}(S_j) \exp 2\pi i (C_j - 1)z] \exp 2\pi i S_j x\}$$

substituting $\bar{F}(S)$ the angular spectrum $\bar{G}(S_j, z)$ becomes:

$$\bar{G}(S) = 1 + i\phi_0 \exp 2\pi i (C - 1)z$$

$$= 1 - \phi_0 [\sin 2\pi (C - 1) z + i \cos 2\pi (C - 1)z]$$

$$2.8$$

The first term represents the carrier. The second term is real and so is in phase with the carrier. It will therefore produce amplitude variations across the wave front. The imaginary term is in phase quadrature with the carrier and so represents phase modulations on it. The terms "amplitude components", and "phase components" of the angular spectra will be used rather loosely to refer to terms in phase or phase quadrature with the carrier respectively. Using this interpretation, the real and imaginary parts of equation 2.8 indicate that for a given value of z, the power transfers between phase and amplitude components as a function of S through the term $\cos 2\pi Cz$. This represents the varying phase advance as a function of S in traveling a distance z and for $d \gg 1$ can be expressed as

$$\phi = 2\pi (C - 1) z = 2\pi z [(1 - S^2)^{\frac{1}{2}} - 1] \simeq -\pi S^2 z$$

The phase modulation in equation 2.8 disappears for values of n such that $\pi S^2 z = (2n - 1)\frac{\pi}{2}$, or $S = [(2n - 1)/(2z)]^{\frac{1}{2}}$.

What this means is that for $S \ll 1/(2z)$, only phase effects
will be present, but amplitude components will dominate the
angular spectrum as S approaches the case for n = 1. There-
fore for screen periodicities d near

$$d = \frac{1}{S} = [\frac{2z}{2n - 1}]^{\frac{1}{2}} \qquad n = 1, 2, \ldots \qquad 2.9$$

The phase modulations produced at the diffracting medium
will appear as amplitude variations at a distance z, which
will tend to produce nulls in any phase spectrum for the
conditions of equation 2.9. The nulls will not be very
sharp due to the motion of the satellite causing variations
in the effective height of the diffracting layer with
latitude. There is also the change in z_1, z_2, and h_o with
zenith angle. Both these effects tend to change the values
of d for which the nulls occur and therefore produce shallow
nulls. Only the first null will have much chance of being
observable due to its large separation from the second null.
The case for $S \ll 1/(2z)$ will be of primary concern in any
study of phase fluctuations because for a thin screen under
this restriction the pattern on the ground is a simple pro-
jection of the screen.

Until now it has been assumed that the source is at
an infinite distance from the diffracting screen. The
actual case is a source at a finite distance. As was shown
by Briggs and Parkin (1963) the change is accomplished by
replacing z by $z_1 z_2/(z_1 + z_2)$, where $z_1 = h_i$, $z_2 = h_o - h_i$

shown in figure 1. This yields the following expression
which replaces equation 2.8:

$$\overline{G}(S,z) = 1 - \phi_o \sin[2\pi(C - 1)z_1 \frac{z_2}{h_o}]$$

$$+ i\phi_o \cos[2\pi(C - 1)z_1 \frac{z_2}{h_o}]$$

<div align="right">2.10</div>

For z_2, $h_o \gg z_1$, equation 2.10 approaches 2.8 since
$z_2/(z_1 + z_2) \rightarrow 1$, but as z_1 increases w.r.t. z_2 the ratio
z_2/h_o decreases until for $z_1 = z_2$, $z_2/h_o = 1/2$. This ex-
treme case won't occur for the restricted zenith angles
encountered in our experiment but ratios on the order of $\frac{7}{10}$
could occur. The effect this has on equation 2.9 is to
lower the sizes of d for which nulls occur by the factor
$\sqrt{z_2/h_o}$ to produce

$$d = [\frac{2z_1}{2n - 1} (\frac{z_2}{h_o})]$$

<div align="right">2.11</div>

2.3   Strongly Refracting Medium

Previously only weak scattering was examined. It
will be shown that there is also the need for considering
cases other than $\phi_o \ll 1$. The consequence of this
inequality not holding is seen most clearly by looking at
equation 2.1. For amplitude effects ($\phi(x,y) = 0$) there is
a linear relationship between $f(x,y)$ and $A(x,y)$ independent
of the size of the amplitude fluctuations imposed by the
medium. This will allow A to be broken into its Fourier

components and $\overline{f}$ to be constructed by the superposition of
the wave fields of the individual components. For a phase
screen a linear relationship doesn't in general hold between
$\overline{f}$ and ϕ and therefore will not allow the superposition
principle to be applied. Letting A = 1 and treating the
one dimensional case, equation 2.1, with $\phi(x)$ broken into
its Fourier cosine series, becomes

$$\overline{f}(x,0) = \exp\{i \sum_{n=0}^{\infty} \phi_n (\cos \frac{2\pi nx}{d})\}$$

$$= \exp \{i[1 + \sum_{n=1}^{\infty} \phi_n (\cos\frac{2\pi nx}{d})]\}$$

Linearity can only be assumed if $\Sigma\phi_n$ for all the screen
components is << 1, for then the exponential can be expanded
into the form

$$\overline{f}(x,0) = 1 + \sum_{n=1}^{\infty} i\phi_n \cos \frac{2\pi nx}{d}$$

There is therefore a need to treat the case for $\phi_0 \gtrsim 1$ dif-
ferently. As will be shown later, this case will occur
more often for large structure sizes in the diffracting
medium. For the larger structures the distance z_1 is such
that simple ray optics can be applied. To a first order
approximation, the phase pattern on the ground will be a
direct projection of that leaving the medium. This is the
same as for the smaller structures which obey the limit

ϕ_o << 1, and thus allows a consistent interpretation for both cases.

For the sake of completeness, the case for $\phi_o \gtrsim 1$ will be looked at in the same manner as that for ϕ_o << 1 to show the consequences of this limit not holding. Using equation 2.7 and applying standard phase modulation theory, $\overline{f}(x,0)$ becomes:

$$\overline{f}(x,0) = \sum_{n=-\infty}^{\infty} (i)^n J_n(\phi_o) \exp\left(2\pi i n \frac{x}{d}\right) \qquad 2.12$$

with $\overline{F}(S)$ comprising components at $S = 0, \pm \frac{1}{d}, \ldots,$ $\pm \frac{n}{d}, \ldots,$ and amplitudes $(i)^n J_n(\phi_o)$. For $n > \phi_o$ the $J_n(\phi_o)$ terms become very small and can be neglected, leaving $2n$ significant spectral components. The effect of these higher order terms will be an increased weighting of the higher components of the power spectrum over what would be expected from weak diffraction theory. Due to the small angles of diffraction for these large structures, only the first few components from a particular point on the screen will be observed, and the components refracted from other parts of the screen won't reach the observer. For non-linear effects of this nature, the presence of more than one periodic pattern in electron density will not produce simply additive phase spectra, but will contain also the additional cross terms for $S = m/d_1 \pm n/d_2$, where m, n are the orders of the terms in equation 2.12.

2.4   Characteristics of the Inhomogeneous F-region

Some important characteristics of the inhomogeneous F-region must be considered if the phase power spectrum it produces are to be analyzed properly.

Previous experimental work has determined some physical properties of the F-region inhomogeneities. By using spaced receivers, (allowing the construction of a two dimensional correlation function in the plane of the receivers) the shape of the correlation contours of the irregularities were found to be ellipsoidal, with the major axis aligned with the local geomagnetic field. Detailed observations of amplitude scintillation performed at Boulder, Colorado (49 degrees N. latitude) produced the following characteristics (Jespersen, Kamas 1963):

r_o = transverse dimension; $0.50 \text{ km} \leq r_o \leq 2.90 \text{ km}$; mean $r_o \simeq 1 \text{ km}$

ΔN_o = total electron variation which increases sharply for northern latitudes, $\geq 40°N$.

H = height of the irregularities; mean H = 325 km

T = thickness of the region; T = 120 km

This description is based on amplitude scintillation data, however, and biased significantly by the diffraction process as discussed above.

It has been shown (Dyson 1969, Kelleher 1970) that the irregularities extend to heights much greater than the average height. It is only because the fairly concentrated band of irregularities near 300 km produces the greatest variations in electron density (peak density of the F-region)
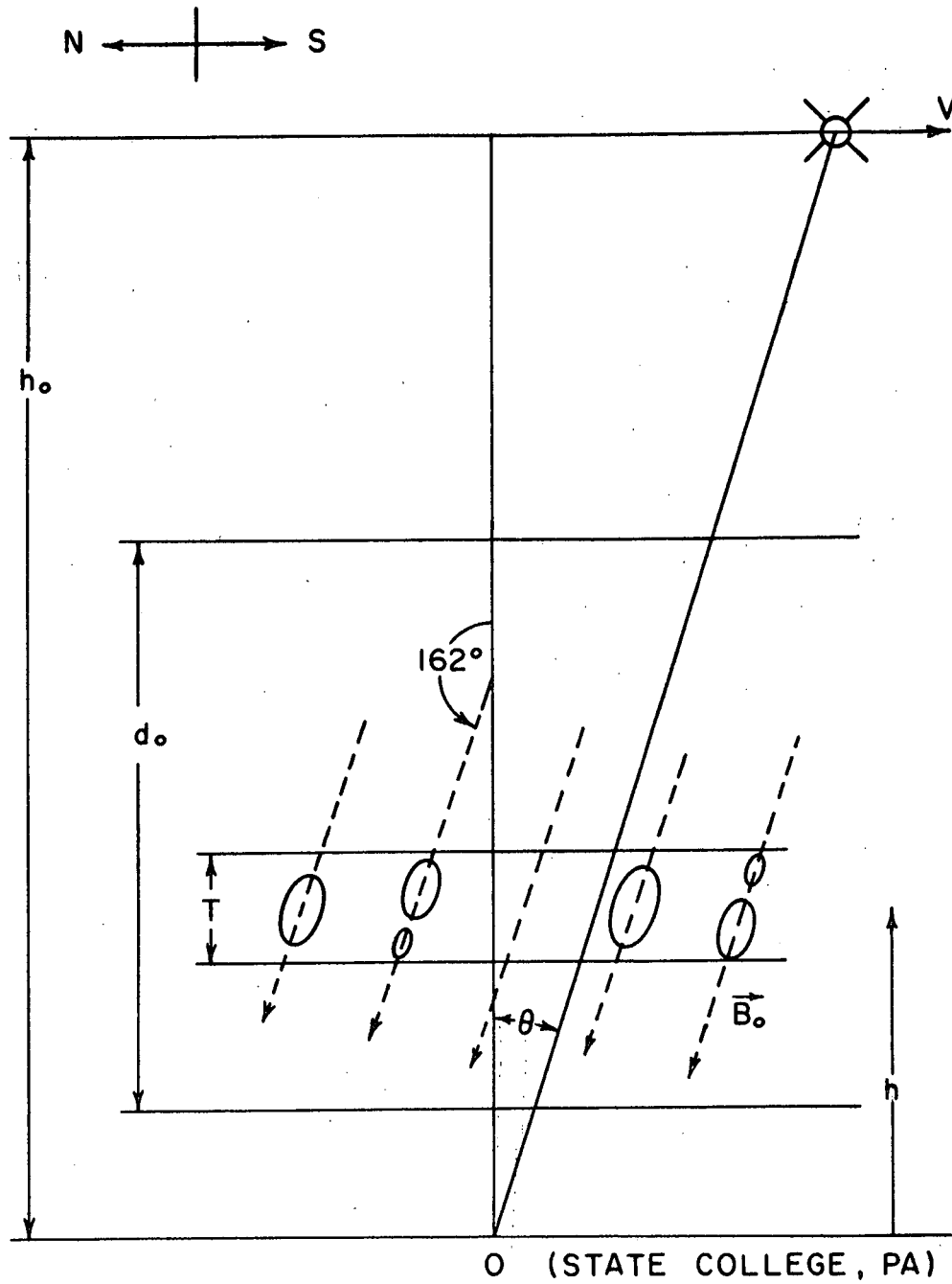
Figure 1   Flat earth geometry of the satellite, ionosphere, receiver system

that the thin diffracting screen approximation can be used.
It is also accepted that the axial ratio ranges from 1 to
10, with an average of about 3.

Some geometrical parameters will be brought in now
for later use in Chapter 4. Because the Beacon B satellite
is in a polar orbit, the ray path of its signals will sweep
along the major axis of the field aligned irregularities for
overhead passes. At the point of observation, 40.8 degrees
N. latitude, the magnetic field has a dip angle of 72 de-
grees. For overhead passes the propagation vector $\hat{k}$ will
therefore be parallel to $\vec{B}_o$ (geomagnetic field), for the
case where the satellite is at its southern most point of
observation (zenith angle of $\simeq$ 23 degrees). As the satellite
progresses northward this angle increases to a maximum of
about 40 degrees. As found by Jespersen and Kamas (1963),
the mean ionospheric height, thickness of the diffracting
medium, and frequency of occurrence of irregularities all
increase with latitude.

2.5   Diffraction by an Inhomogeneous Ionosphere

Due to the lack of amplitude information in the
recorded data (see Chapter III), it will not be possible to
produce an exact description of the phase power spectra
leaving the diffraction medium, rather a qualitative
description of the general shape of the lower end of the
expected spectra will be sought.

The power spectrum of the phase modulation

$P_\phi(k_x, k_y)$ imposed upon the signal near a thin diffracting screen and the power spectrum of electron density fluctuations $P_N(k_x, k_y, k_z = 0)$ are related by

$$P_\phi(k_x, k_y) = 2\pi(r_e\lambda)^2 L P_N(k_x, k_y, k_z = 0) \qquad 2.11$$

(Lovelace et al. 1970, Cronyn 1970).

$\quad$ L = thickness of the diffracting region

$\quad r_e$ = classical electron radius = 2.83×10^{-15} m

$\quad \lambda$ = wavelength of the signal

$\quad k_j$ = spatial wave number in the j direction

$\quad k_z$ = 0 was chosen to represent a thin diffracting medium.

The shape of the two spectra are similar and thus represent a simple projection of the electron density variations of the medium on the wavefront in the form of phase fluctuations. It has been observed (Porcello and Hughes, 1968) that the form of P_N for the case of auroral zone inhomogeneities can be given by a power law variation of the form:

$$P_N(k_x, k_y, k_z = 0) = A(k_x^2 + k_y^2) - \frac{\beta_H + 1}{2}$$

with β_H found experimentally to range from 3 to 4.

$\quad$ A check on the validity of the assumption $\phi_0 \ll 1$ will now be made. The phase deviation in traversing the medium is given by:

$$\phi = - r_e \lambda \int_0^\ell \Delta N dl$$

where r_e is the classical radius of the electron. Letting the deviation in electron density ΔN be Gaussian, $\phi(x)$ becomes (as shown in Briggs and Parkins 1962)

$$\phi(x) = - r_e \lambda \sqrt{\frac{\pi}{2}} \frac{-\Delta N\, r_o}{\sin \psi} \exp[- \frac{2x^2}{r_o^2}]$$

with typical values to be expected

ψ = angle between $\vec{B}_o$ and $\hat{k}$ = 20 degrees

ΔN_o = maximum electron density change = 1.0% of $10^{11} \frac{1}{m^3}$ = $10^9 \frac{1}{m^3}$

λ = 15m

α = axial ration of the ellipsoid = 5

r_o = 5 km

$$\phi(x) = 8.3 \times 10^{-2} \exp[-2(\frac{x}{10^3})^2]$$

This gives a maximum phase shift of $\phi(0) \simeq 0.5$ radians. It is therefore conceivable that for larger structures, r_o = 50 km, and larger electron density variations ΔN_o = 10%N_o, values of ϕ could be on the order of 50 radians. Thus we could expect higher order components along with the first order term. The number of side components n is roughly n = ϕ. If we use the value of $10^9 \frac{1}{m^3}$ for ΔN_o, the largest irregularity for which ϕ_o < .25 radians can be found to be

$$.25 = 8.3 \times 10^{-2} \frac{r_o}{10^3 m}$$

$$r_o = 3.0 \text{ km}$$

If it is assumed that ΔN_o is proportional to r_o, there will be a cutoff at which the approximation $\phi_o << 1$ no longer occurs. It is therefore expected that the power contribution to the high end of the observed phase spectrum will contain the sum of contributions from the short periodicity screens and also the higher order components of those large structures which lie below the cutoff.

Using equation 2.11 the amplitude effects aren't significant for $d >> [2z_1(z_2/h_o)]$. For $\lambda z_1 = 300$ km, $\lambda z_2 = 700$ km this condition becomes $d >> 3$ km to yield a lower bound on structure size, above which the phase pattern produced at the ground is a simple projection of the pattern at the diffracting medium. This cutoff will be chosen to be 5 km.

Due to satellite motion the 2-dimensional spatial diffraction pattern at the ground has a velocity $V = - h_i V_s / (h_o - h_i)$. Because of this motion an observer at a single receiving station will observe a one dimensional temporal scan of this pattern, assuming that it moves without change. This assumption is equivalent to assuming that the diffracting region is very thin in vertical extent. The spatial wave numbers of the pattern k_j can be equated to the

temporal frequency components f_j by $k_j = 2\pi f_j/V$ or $k_j = 2\pi f_j(h_o - h_i)/(h_i V_s)$ to produce $k_j = 2.09 \ f_j$ sec/km. The power spectrum in frequency of the received temporal pattern can therefore be used to reproduce a one dimensional spatial pattern.

CHAPTER III

SIGNAL HANDLING AND DATA REDUCTION

EQUIPMENT AND TECHNIQUES

3.1   Source and Initial Signal Handling

The source used was the S-66 Ionospheric Beacon-B
Satellite with the following orbital parameters:

Nodal Period	104.8 minutes
Inclination	79.7 degrees
Perigee	890 km
Apogee	1070 km

It produces continuous, harmonically, related
signals at the frequencies 20, 40, 41, MHz (NASA 1963). Use
will be made of one of the circularly polarized modes of the
20 MHz signal and the linearly polarized 40 MHz signal.

The receiving and recording equipment was construct-
ed about 8 years ago by previous workers, with the block
diagram shown in figure 2. The data was collected over the
period 1964-1968, and after processing was stored on mag-
netic tape. The signals were also recorded on chart records,
a sample of which is included in Appendix B. By using har-
monics of a single tracking oscillator for both frequencies,
the phase relationship between them was preserved for later
phase comparison. The receiving antennas consist of a fixed,
vertically directed, circularly polarized antenna and a
fixed dipole with an east-west orientation.

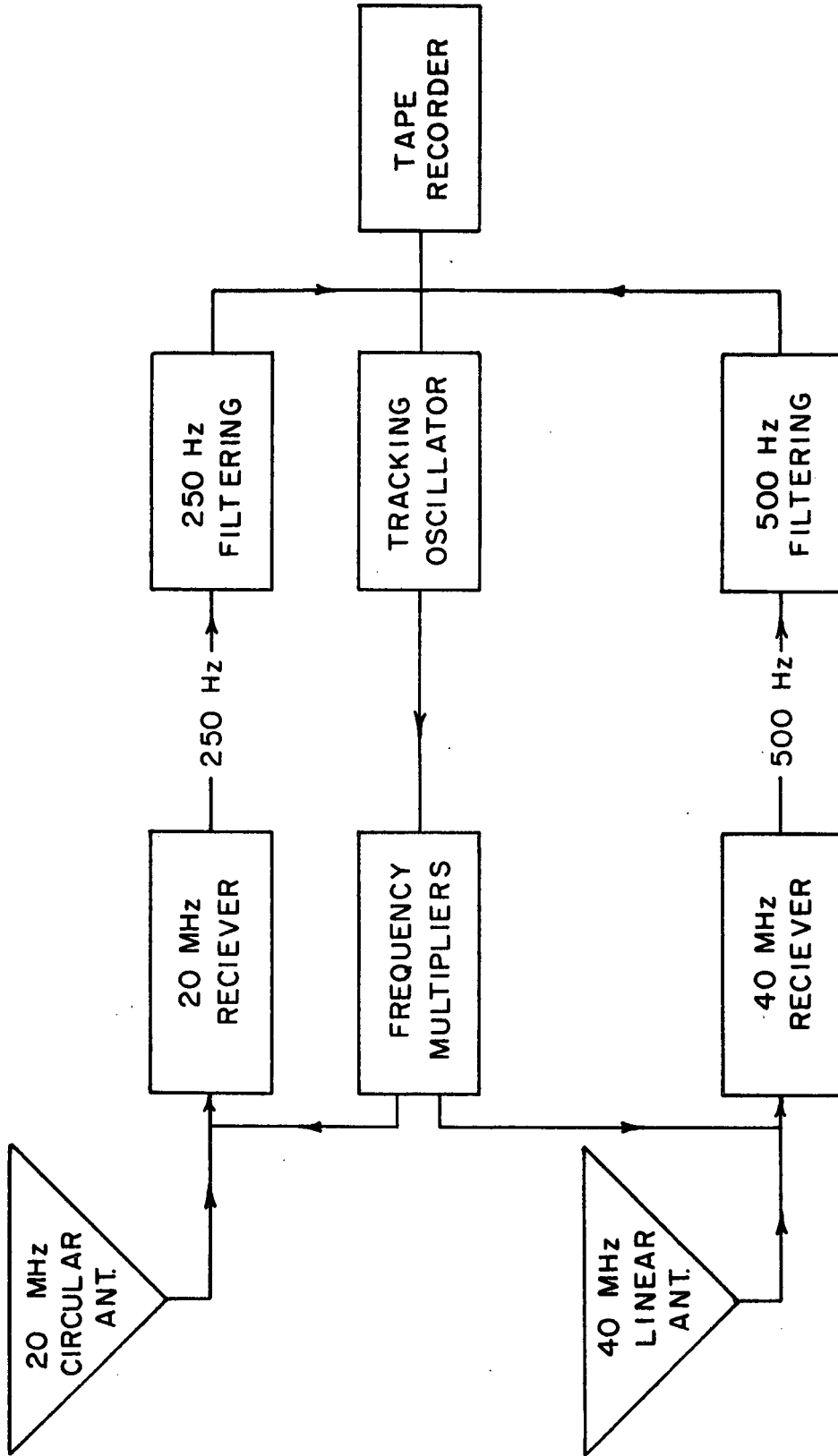The direction of polarization of the incoming

C

Figure 2   Block diagram of the receiving equipment

signals will change with time to produce a Faraday rotation rate. This is caused by the systematic change in ionospheric thickness and in the longitudinal component of the earth's magnetic field with zenith angle. For the single dipole antenna this produces severe amplitude variations which must be compensated for in the early stages of the electronics due to the critical signal level dependence of the phase detection circuitry. There will also occur phase discontinuities at the times of cross-polarization between the incoming wave and the antenna. These discontinuities will produce spikes in the temporal diffraction pattern and therefore produce a spurious addition to the phase spectra. Because the 20 MHz circularly polarized antenna was fixed it will appear to be ellipitically polarized for oblique incidence of the signal. This will produce an apparent, non-uniform Faraday rotation rate which in turn produces phase modulations. The magnitude of this effect is increased with increasing zenith angle which makes necessary the limiting of satellite longitudes to the range 75-80 degrees west and of latitudes to the range 35.5-46.5 degrees north. Since the above effects are reduced by a decreased Faraday rotation rate which is dependent on the integrated electron density of the ionosphere, only night time records will be used.

A brief note will be added here as to why linear, rather than circular polarization was used for the 40 MHz signal. Both 20 and 40 MHz circularly polarized signals

were stored on the same tape channel. There was some distortion in the receiving equipment which generated a second harmonic of the 250 Hz stored signal. This harmonic was inseparable from the 500 Hz signal, and caused spurious phase modulation of it.

3.2   Analog Processing

The approach used is to compare the frequencies of the two previously stored signals yielding a continuous temporal frequency record. This represents the derivative of the temporal phase function w.r.t. time recorded at the receiving station. The frequency record represents the deviation w.r.t. time of the signals from their harmonic relationship, which will give the phase path difference experienced by the signals in traversing any inhomogeneities in the F-region. Utilization of harmonically related signals allows the elimination of tracking errors, source stability errors, and phase noise induced during the recording and playback process. This is accomplished by frequency doubling the 250 Hz signal and comparing it with the 500 Hz signal to eliminate any modulation proportional to frequency, of which all the above produce. The 500 Hz signal was offset by 180 Hz (chosen by trial and error to produce the least harmonic distortion) to facilitate phase detection. A block diagram of the electronics is shown in figure 3, where C.f. and B.W. are abreviations for center frequency and bandwidth respectfully. The following requirements were placed
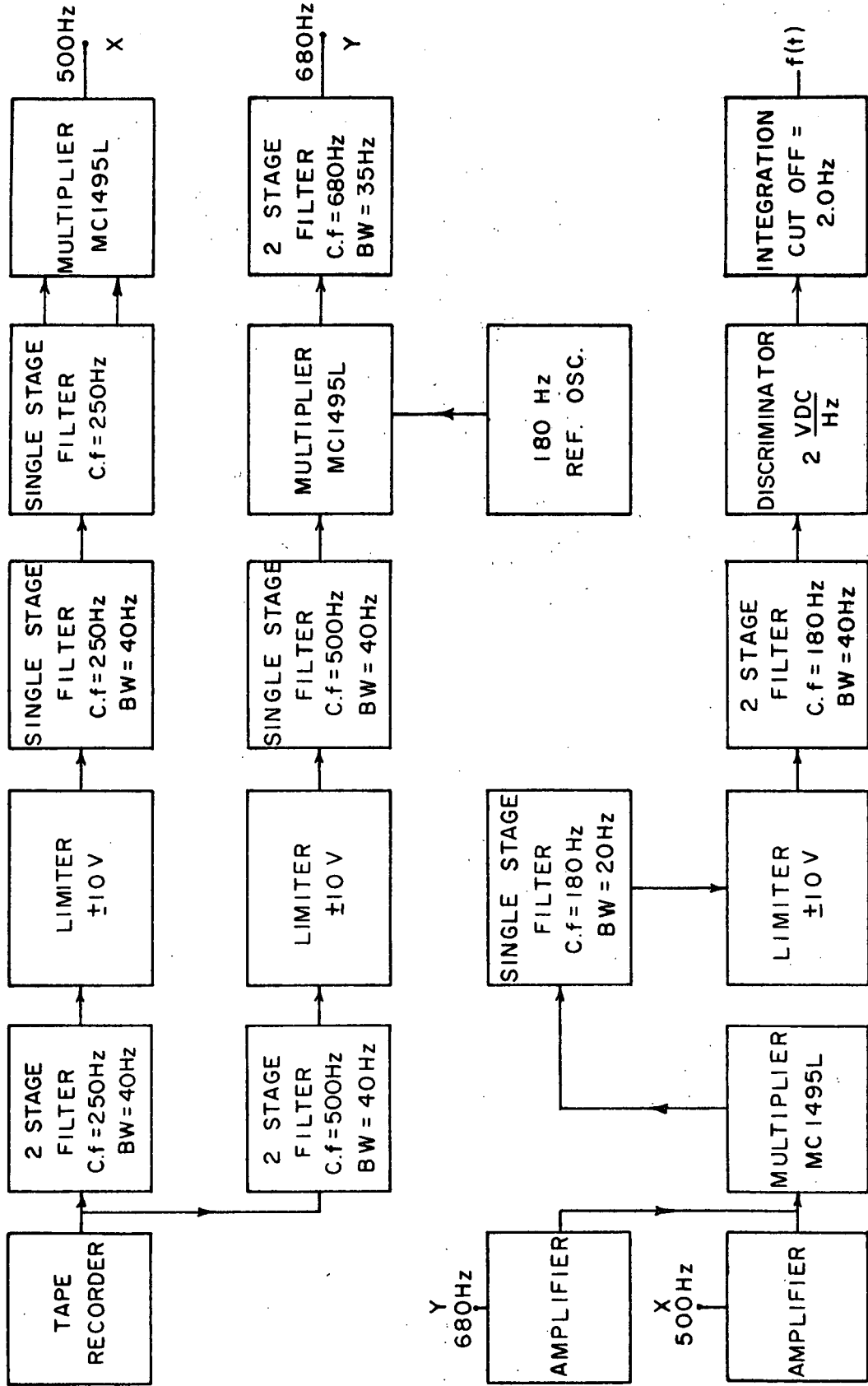
Figure 3 Block diagram of filtering and discriminator circuitry

on the electronics to account for physical conditions and, or previous recording methods.

Because the frequency discriminator used was sensitive to amplitude variations, severe amplitude limiting was imposed prior to frequency detection. This need was made more demanding by the deep nulls in signal caused by Faraday rotation, especially on the 500 Hz signal.

Predetection bandwidth requirements were imposed in early limiting to prevent harmonic distortion from reaching the frequency detector. Minimum bandwidth (B.W.) requirements are set by the phase modulation induced on the signal. Due to the changing effective thickness (shown in figures 1 and 4) of the ionospheric layer with satellite latitude β, we will have a linear ramp imposed on the discriminator output. Hereafter this effect will be referred to as the apparent doppler dispersion. Its magnitude is approximated by:

$$\phi = -r_e \lambda \int_0^\ell N(x)dx \qquad 3.1$$

$$f = \frac{1}{2\pi} \frac{d\phi}{dt} = -\frac{r_e \lambda}{2\pi} \frac{d}{dt} \int_0^\ell N_o dx \qquad 3.2$$

$$= -\frac{r_e \lambda}{2\pi} \frac{d}{dt} (N_o \ell) \qquad 3.3$$

N_o = average electron density (assumed here to be constant)

ℓ = arbitrary ionosphere thickness

(a)

$$\text{Sin}\left[\text{Tan}^{-1}\left(V_s\,\beta\,/\,18h_o\right)\right] \text{ vs. } \beta$$

(b)

$$f(\beta) \text{ vs. } \beta \qquad f(\beta) = \text{Sin}\,\beta\left[\text{Cos}\,\beta\,(r_i^2+r^2-rr_i\,\text{Cos}\,\beta)-rr_i\right]\left[1-\left(\text{Sin}^2\beta/\,r_i^2+r^2-2\,r\,r_i\,\text{Cos}\,\beta\right)\right]^{-3/2}$$
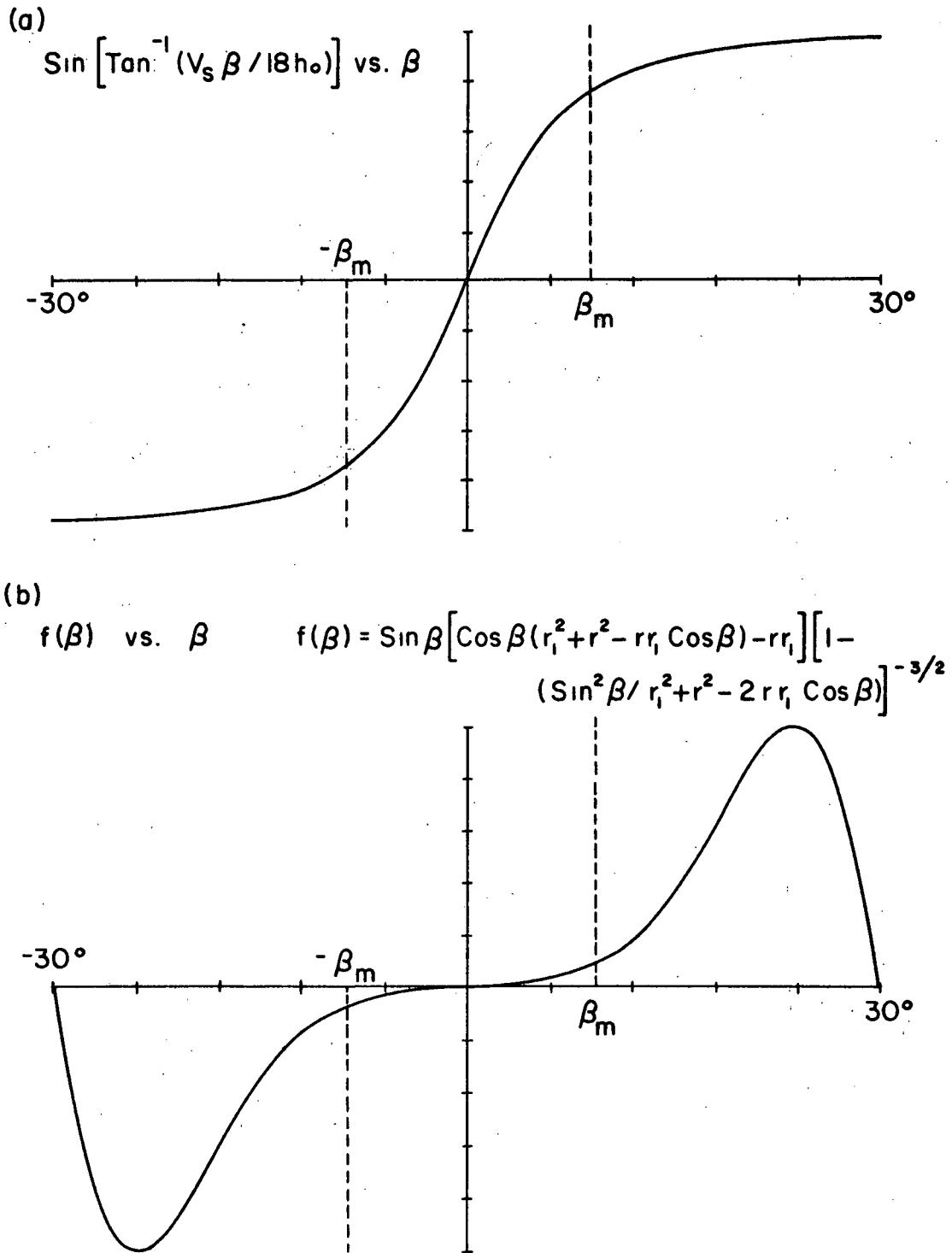

Figure 4   Frequency modulation caused by the apparent doppler dispersion for (a) flat earth, (b) curved earth geometry. $R_e \equiv$ radius of the earth, $r = (R_e + h_i)/(R_e + h_o)$, $r_1 = (R_e + h_i)/R_e$, $\beta_M =$ maximum β of observation

and becomes

$$f = - \frac{r_e}{2\pi} \lambda N_o V \frac{d_o}{h_o} \sin \theta \qquad\qquad 3.4$$

The records were restricted to values of $\theta \leq \theta_m =$ 23°. Using nighttime values of N_o given by Solomon (1965), the maximum frequency deviation for the frequency doubled 250 Hz signal at the extreme zenith angles of the data was found to be $f_{max} \simeq \pm 0.5$ Hz for the 20 MHz signal. Because both the 20 and 40 MHz signals are modulated by the iono- sphere similarly but with different magnitudes, $\lambda_{20} - \lambda_{40}$ should have been used rather than λ_{20} which reduces f_{max} to about ± 0.4 Hz.

The tracking errors were measured by previous workers to be as large as 10 Hz and must be considered in B.W. considerations of the filtering prior to the mixing of the two signals. Because the analysis treats ionospheric induced frequency modulations up to 3 Hz, (actually up to 8 Hz, but this region wasn't analyzed because of severe attenuation due to postdetection filtering) this will have to be added into both predetection and postdetection B.W. limits. Combining the above, the predetection B.W. needed is 2(10+3+0.5)Hz = + 27Hz. It was set to 30 Hz. Post- detection integration contained a cutoff at 2 Hz.

The discriminator output represents the frequency difference of the 2 signals as a function of time. This necessitates that the delay of each signal through the

electronics be identical, i.e., that the rates of change of phase shift vs. frequency for each signal channel be equal. This was achieved with an additional filter in the 250 Hz channel to yield slopes differing by less than 5%, representing a phase error of ten degrees for a frequency change of 28 Hz.

Because the discriminator used was very sensitive to amplitude variations, severe limiting was used and signal amplitude was monitored to insure against fluctuations. Discriminator output remained constant for the following ranges of signal input:

Amplitude 250 Hz: $0.6 \leq V(250) \leq 3.2$ VP-P

Amplitude 500 Hz: $0.2 \leq V(500) \leq 3.2$ VP-P

The discriminator output was placed through a 3 stage, low pass, filter with cutoff at 2.0 Hz.

Its response was linear over the range used ($\pm$ 5 Hz) with a sensitivity of $2\frac{VDC}{Hz}$ and a noise level (due primarily to intermodulation in the earlier electronics) of $\pm$ .02 Hz.

A sample of a typical chart record produced by the above is shown in figure 5. This information consisted of:

Channel 1: WWV

Channel 2: discriminator output f(t) in Hz

Channel 3: discriminator input amplitude monitoring

Channel 4: 40L amplitude monitoring

3.3   Data Analysis

The aim of this stage of analysis is to obtain a

Amplitude of 40 MHz Signal Linear Polarization

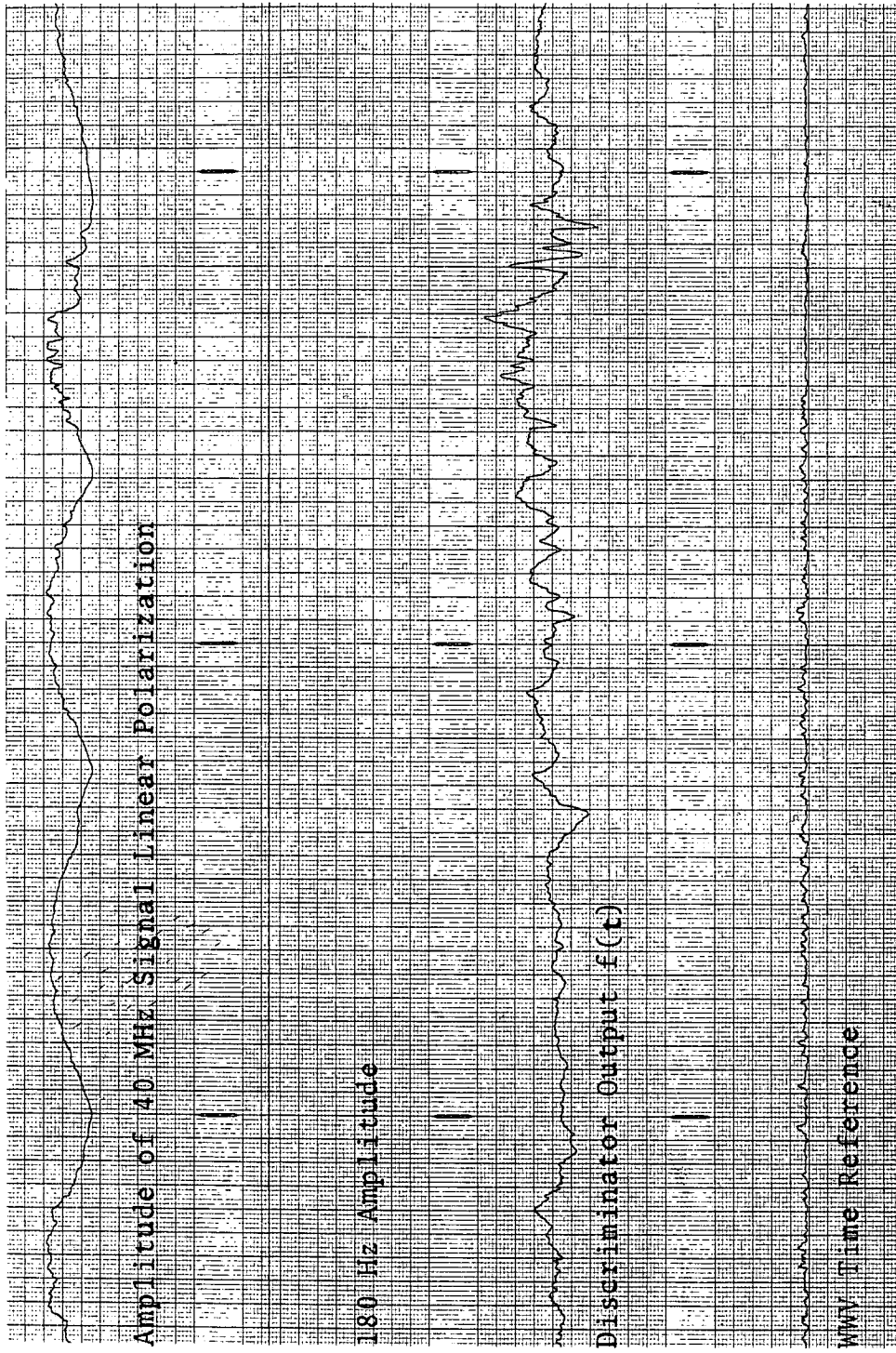180 Hz Amplitude

Discriminator Output f(t)

WWV Time Reference

Figure 5   Sample Record of Discriminator Output f(t).

power spectrum of the phase variations imposed on the received signal. The method used is outlined by Blackman and Tukey.

To avoid the complexity required to obtain the frequency components by analog methods, the data will be digitized. This action replaces the continuous function $f(t)$ by $f(t_j)$, where t_j represents the discrete time values $j\Delta t$, $j = 1,2 \ldots N$, $N\Delta t$ = length of the record. As noted earlier, there exists a D.C. trend on the data. To eliminate this large, low frequency contribution, the best linear fit line was subtracted from the data point by point. Determination of the line defined by the quantity $(\alpha + \beta j \Delta t)$ was achieved by the use of:

$$\sum_{j=1}^{N} [f(t_j) - \alpha - \beta j] = 0 \qquad 3.5$$

$$\sum_{j=1}^{N} (j - \frac{N}{2}) [f(t_j) - \alpha - \beta j] = 0 \qquad 3.6$$

Solving for α and β, the trend and mean can be subtracted out. The autocorrelation function of the detrended data was found, and its Fourier transform taken, yielding the power spectrum in frequency, which will be shown later to be related to the power spectrum in phase. Several aspects of digitizing data must be considered before the usefulness of the data can be assured.

Computation was performed on a PDP-10 digital computer with a limit of 23 k user available core. This set

a practical upper limit on the size of the data array and therefore the sampling rate. Because the maximum observable frequency with a sampling rate of N per second is 1/(2N), N was set so 1/(2N)=8 Hz. The data was already limited to $\lesssim$ 3 Hz due to final filtering, so no loss of information occurred. N therefore is equal to 16 samples per second. Previous work (Porcello and Hughes, 1968) has shown the power spectra to fall off with increasing frequency which will further reduce aliasing. The longest lags obtained are determined by the length of the record, and are usually taken to be 5-10% of the record length. We chose lags up to 32 seconds which is $\approx$ 16% the record length. This gain in range of data is seen in equation 3.7 to reduce the stability of the results (represented by K).

Maximum aliasing is determined by the attenuation of the output filter. The power at the folding frequency of 8 Hz is compared with that at 0 Hz and was found to be down 68 db. This is more than sufficient to eliminate any aliasing problems.

Due to changing ionospheric conditions between orbits, nonstationarity between records is assumed, which forces statistical independence of the records, rather than an average over an ensemble. For the record length available and maximum lag used, the number of degrees of freedom, K, is found to be (Blackman and Tukey):

$$K \simeq \frac{2T_n'}{T_m} = \frac{2[T_n - 1/3T_m]}{T_m} \qquad\qquad 3.7$$

$$T_n = \text{total record length}$$

$$T_m = \text{maximum lag desired}$$

$K = 11\text{-}1/3$. Use of Table II in Blackman and Tukey leads to an 80% confidence limit of 4.8 db. This value is only characteristic of the runs taken, with exact values given later for individual records.

Past evidence (Porcello and Hughes, 1968) has shown the phase spectral density to follow a power law relationship, given by

$$P_\phi (k_x, k_y) \propto (k_x{}^2 + k_y{}^2)^{-\frac{\beta_H + 1}{2}}$$

with k_x, k_y the wave numbers and β_H an experimentally determined variable. This indicates the need for prewhitening. The data being originally intended for other uses, prewhitening wasn't performed. This will reduce the signal to noise ratio at the high end of the spectrum, making that region more susceptible to interference or noise.

The process of taking a finite sample is equivalent to multiplication of the infinite data set with a square pulse. This will accentuate the high frequency end of the spectra. This effect was reduced by passing the auto-correlation function $C(T_j)$ through a Hamming spectral window $D(T_j)$ where

$$D(T_j) = .54 + .46 \cos(\pi T_j/T_m) \qquad |T_j| \leq T_m$$
$$= 0 \qquad\qquad\qquad\qquad |T_j| > T_m$$

The attenuation due to final integration was compensated for by direct measurement of the characteristics of the low-pass filter and multiplication of the frequency power spectra lines by the appropriate value.

The flow diagram and computer program are included in Appendix A-2.

CHAPTER IV

EXPERIMENTAL RESULTS

4.1   Experimental Details

The individual orbital conditions and statistical parameters of the data used are given in Table I. Due to the severe limitations on longitude and the restriction to nighttime records, only a small fraction of the available library of records was considered of which only 8 satellite passes produced significant frequency variations observed at the discriminator output. The effectiveness of the trend removal performed on the digitized discriminator output was about a 10^6 reduction in mean value, and a 10^7 reduction in slope. Because both the original mean and trend were of the same order of magnitude as the desired information, these reductions brought their effect well below the noise level. For an 80% confidence limit, there was typically a 5 db uncertainty range in the relative power spectra.

A sample of the discriminator output is shown in figure 5. The 40 MHz amplitude channel was displayed so as to observe the magnitude of the frequency spikes produced by the Faraday rotation and any possible amplitude effects it could cause. These finite width spikes have a minimal overall effect on the spectra due to their infrequent occurrence. The scale is 1.0 Hz per division on the discriminator channel.

TABLE I: ORBITAL PARAMETERS AND EXPERIMENTAL RESULTS

Orbit No.	Time (LMT) 0° Zenith	Longitude of Satellite 0° Zenith	Duration of Record (Sec.)	No. of Degrees of Freedom	Range in db for 80% Confidence Limit	β
10566	2239.11	80.2	232.0	13.8	4.47	1.5
6173	0525.44	80.3	243.7	14.6	4.34	0.82
6378	0332.26	81.8	244.1	14.6	4.34	0.50
8468	0622.04	78.8	161.2	9.41	5.17	0.81
8550	0536.26	80.8	195.3	11.5	4.93	0.66
9356	2132.15	79.4	157.8	9.2	5.24	0.76
9397	2109.11	79.6	164.4	9.6	5.11	0.75
5962	2023.43	74.9	244.0	14.6	4.34	0.64

4.2   Spectral Density of the Frequency Modulation

(a)   Analysis of the high end of the spectra.

Sample plots are shown on log-log scales in figures 6-11. Figures 6 and 7 show a spectrum before smoothing and after smoothing. Smoothing was accomplished by taking a running average over three unsmoothed logarithmic spectral values, which themselves were arithmetic averages over two adjacent spectral values. The remainder of the figures are for smoothed plots only. This doesn't reduce the useful information because as is seen in figure 6 the features present in the unsmoothed version and not in the smoothed version are within the range of uncertainty imposed by the 80% confidence limit shown on each graph. The consistent appearance of nulls at the high end of the spectra is a feature to which attention is now drawn.

For a source at a finite distance from the observer it was predicted in equation 2.10 that nulls in the power spectra of structure sizes should occur for dimensions given by equation 2.11. A conversion from spatial to frequency spectra produce nulls for frequencies

$$f = \frac{V_s}{D} \frac{h_i}{h_o} = \frac{V_s h_i}{h_o \lambda d} = \frac{V_s}{\lambda} \left[\frac{2n - 1}{2} \left(\frac{h_i}{h_o (h_o - h_i)} \right) \right]^{\frac{1}{2}} \quad n = 1, 2, \ldots$$

$$4.1$$

This produces nulls at the frequencies (for $n = 1,2,3, \ldots$ respectively) $f = 0.675, 1.31, 1.69, \ldots$ Hz. Figures 6-11 show definite nulls in this frequency range, but
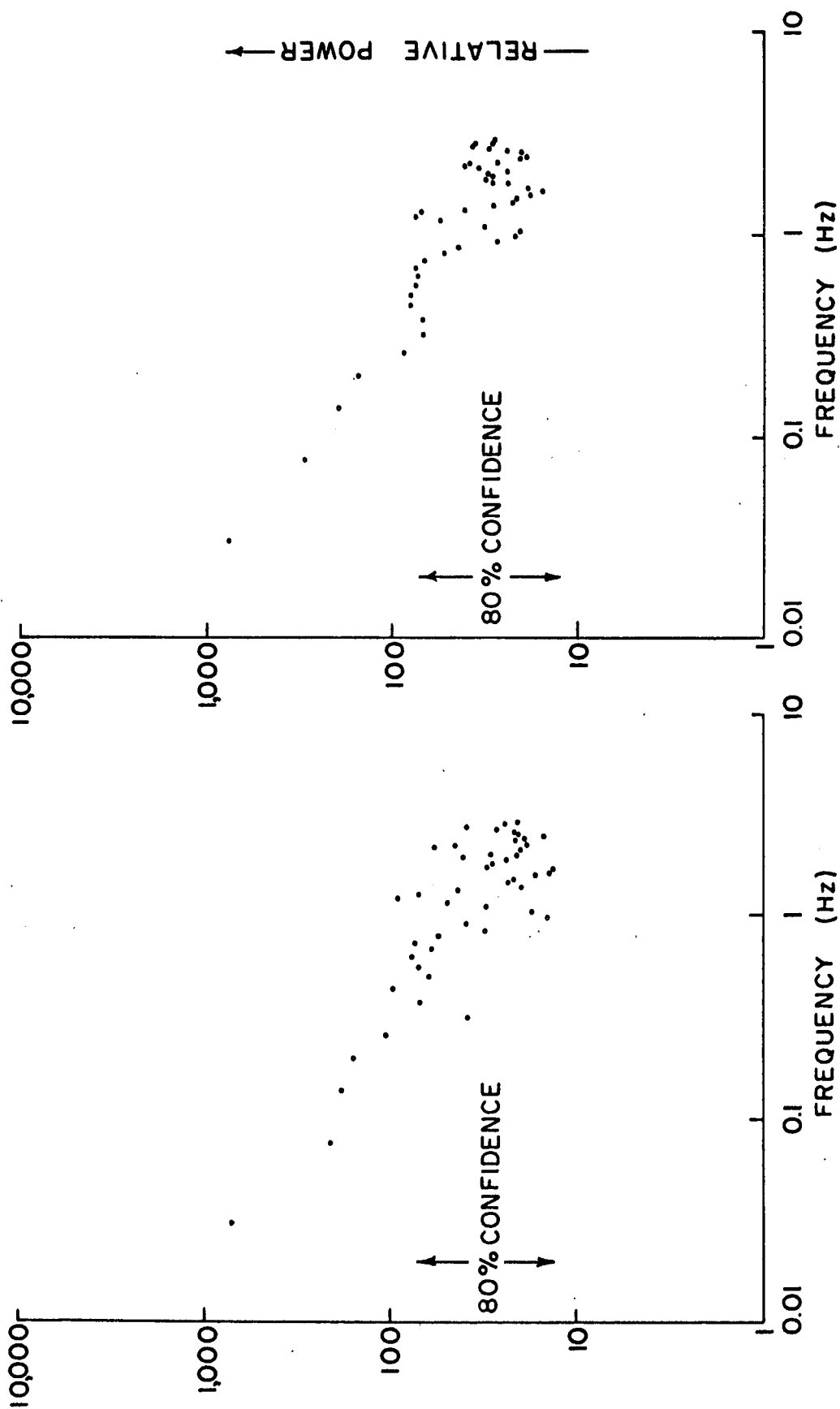
Figure 6   Unsmoothed power spectrum for orbit
           6173

Figure 7   Smoothed power spectrum for orbit
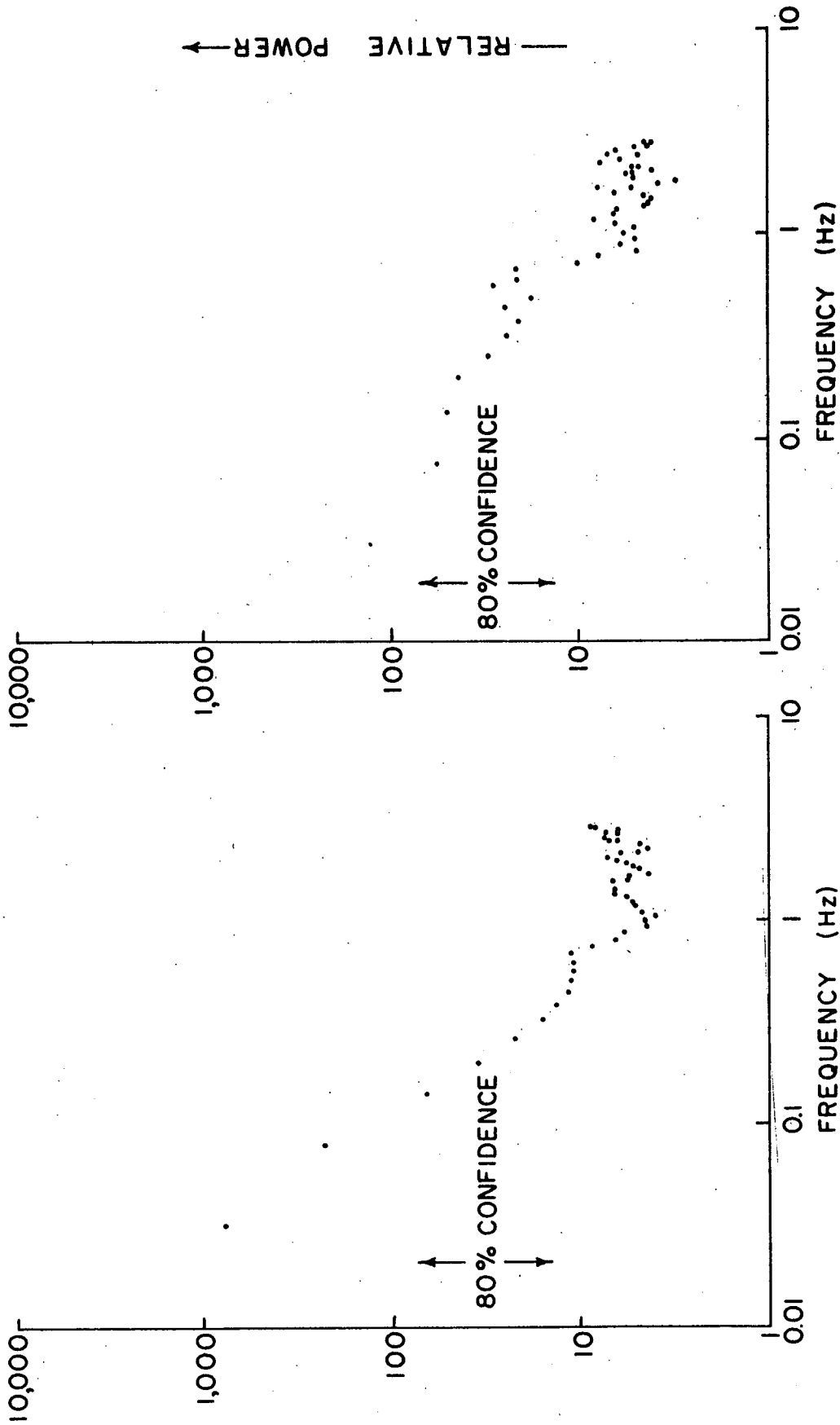   6173

Figure 8   Smoothed power spectrum for orbit
           10566

Figure 9   Smoothed power spectrum for orbit
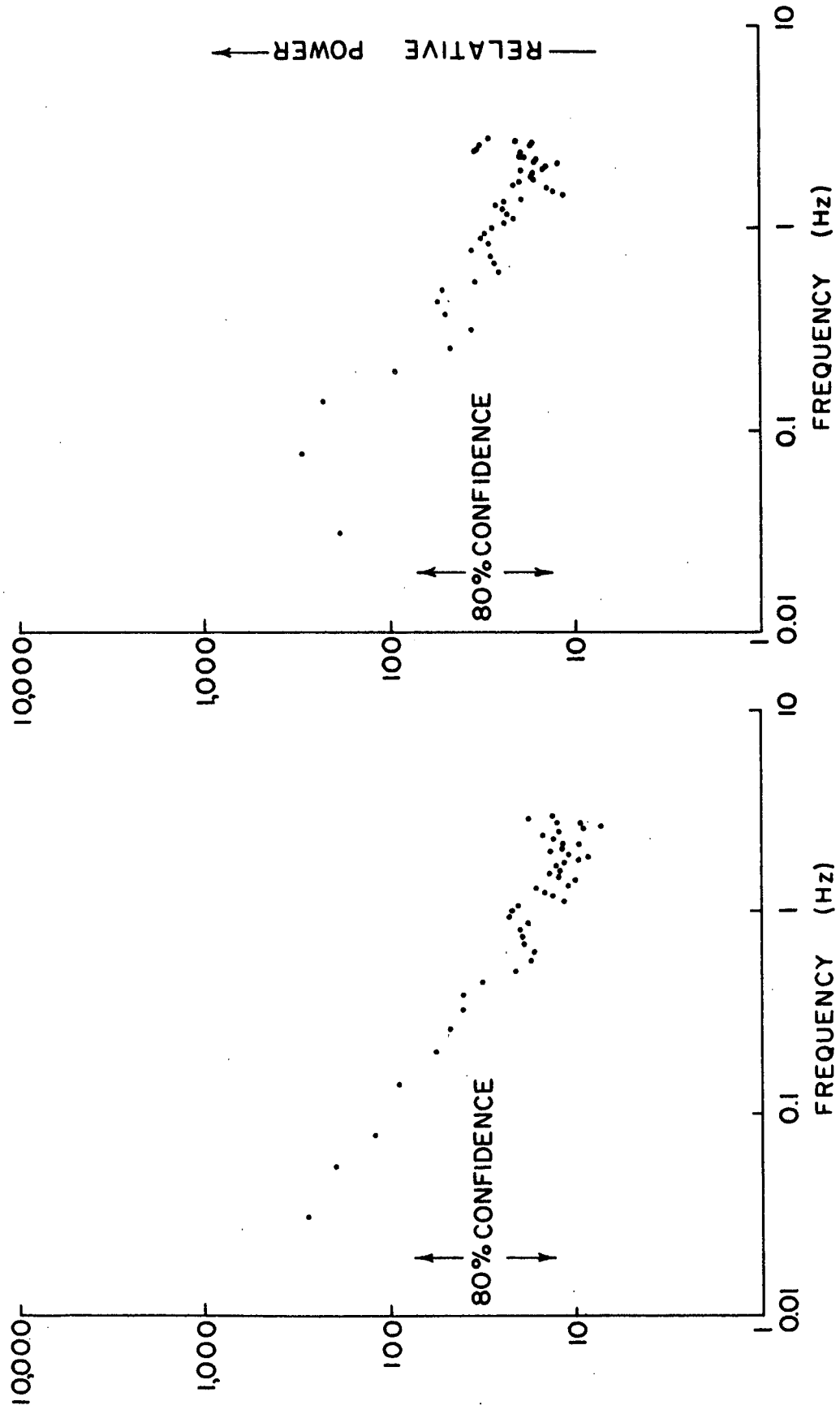   8550

Figure 10   Smoothed power spectrum for orbit
9356

Figure 11   Smoothed power spectrum for orbit
9397

generally not at these precise values.

Upon a closer analysis of the geometry involved, it becomes clear why the predictions above aren't realized. The values of the predicted nulls depend on the height of the diffraction medium and the distance to the satellite. As shown in section 2.4 the medium height increases with increasing latitude and h_o increases with zenith angle. The finite thickness of the diffracting layer also produces inhomogeneities at different heights. Assume for example that h_i varies over the range 300-400 km. This produces a first order null ranging from 0.675 to 0.504 Hz to produce a broad null centered about 0.59 Hz. It could also be the case that there exist diffracting layers at different heights. This effect could come about through a patch structure of inhomogeneities as observed by Kelleher and Sinclair (1959). Here structures appear in groups producing the possibility of patches occuring at different altitudes, 300 and 400 km for example. This would also produce distinct first order nulls at 0.675 and 0.504 Hz.

No quantitative analysis will be made of this region for the following reasons: (1) the confidence limits are of the same order of magnitude as the depth of the nulls, (2) the data is believed to be approaching the system noise level in this region as indicated by the characteristic flattening of the spectra. Had these two conditions not been present, some estimate of the height and thickness of the diffracting medium could possibly have been obtained

from the position and shape of the nulls. It is interesting to note that although the nulls should occur in both amplitude and phase power spectra, amplitude studies (Rufenach 1972) have only rarely observed them, while they are quite evident in this study using phase scintillation.

(b) Analysis of the low end of the spectra.

This is the region of the spectra containing frequencies below the first null. This frequency is found, using equation 4.1 for n = 1 and converting from normalized distances to actual distances, to be

$$f = \frac{V_s}{\lambda} [\frac{1}{2} \frac{Z_1}{Z_2 H_o} \lambda] = V_s [(\frac{1}{2\lambda}) \frac{Z_1}{Z_2 H_o}]^{\frac{1}{2}} \qquad 4.1a$$

It is in this region that some insight might be gained as to the physical nature of the diffracting medium.

From the records studied there tends to be a definite slope β in the log-log plots shown. This would indicate a frequency power spectrum of the form

$$P(f) \propto (f)^{-\beta} \qquad 4.2$$

Upon taking a visual estimate of the slope, it was found to have a mean value of 0.71 and standard deviation of 0.10. These values were found neglecting the β value for orbit 10566 due to its large deviation from the norm. Upon looking at the chart record for this run a considerably larger amount of low frequency variations were present, thus

indicating a greater than average (taken over the 8 passes used) number of larger structure sizes w.r.t. the smaller sizes.

(c) Statistical stationarity of the results.

Due to the similarity of values of β for the different orbits, some support is rendered to the case for statistical stationarity of the medium w.r.t. this parameter. Porcello and Hughes (1968) also found similar values for β for structure sizes smaller than considered here. From the limited sample taken, there is the indication that the parameter is a characteristic of the medium and not dependent upon temporal changes occuring in the inhomogeneous makeup of the diffracting medium. Orbit No. 10566 produced a β value with considerable deviation from the mean value. Because of the limited sample taken, no conclusions will be drawn from this deviation.

4.3 Discussion of the results

It was shown from the graphs and expressed in equation 4.2 that the power spectrum obeys a power law variation with frequency. What is of more physical significance is the power spectrum of the phase difference $\phi(t)$ of the two signals. Noting that $f(t) = d\phi(t)/dt$, the Fourier transform of $f(t)$ is

$$F_f(f) = \int_{-\infty}^{\infty} f(t)e^{-2\pi i f t}dt$$

$$F_f(f) = \int_{-\infty}^{\infty} \frac{d}{dt} \phi(t) e^{-2\pi i f t} dt$$

$$= \frac{1}{i} f \int_{-\infty}^{\infty} \phi(t) e^{-2\pi i f t} dt$$

$$= - i f F_\phi(f) \qquad\qquad 4.3$$

the comparison of power spectrum yields:

$$P_f(f) = |F_f(f)|^2 = f^2 |F_\phi(f)|^2 = f^2 P_\phi(f)$$

$$P_\phi(f) = f^{-2} P_f(f) \qquad\qquad 4.4$$

$$P_\phi(f) \propto f^{-(\beta+2)} \qquad\qquad 4.5$$

It is now desirable to determine the nature of the spatial power spectrum in phase leaving the diffracting screen, denoted by $P_\phi'(k)$. Equation 2.8 shows how the angular spectrum in phase changes as the distance from the screen increases. For the cosine diffracting screen considered previously, the power at the screen is given by

$$P_\phi(S) = |F(S)|^2 = 1 + \phi_o^2 \quad (S = \tfrac{1}{d})$$

On the ground the power contained in the phase part of the angular spectrum is

$$P_\phi'(S) = |G(S)|^2 = \phi_o^2 \cos^2[2\pi(1 - \frac{S^2}{2} - 1)z] \quad (S = \tfrac{1}{d})$$

$$P_\phi'(S) = \phi_o{}^2 \cos^2 \pi S^2 z \qquad\qquad 4.6$$

Expanding the cosine term $P_\phi'(S)$ becomes

$$|P_\phi'(S)| \simeq \phi_o{}^2 (1 - \pi z S^2) \qquad\qquad 4.7$$

Because it has already been assumed that $zS^2\pi \ll 1$, the spectrum is independent of S and identical to that for z = 0. Next the dependent variable in equation 4.5 will be changed from frequency to wave number along the direction of motion k using $k \propto f$

$$P_\phi(k) \propto k^{-(\beta+2)} \qquad\qquad 4.8$$

A proportionality rather than an equality is used due to the nature of measurement of the power spectra. The power spectrum of the electron density fluctuations is therefore

$$P_N'(k) \propto k^{-(\beta+2)} \qquad\qquad 4.9$$

What is obtained therefore is a power law variation in electron density fluctuation over the range of iono- spheric structure sizes 5.0 km to 73 km. The character- istic exponent was - 2.71. Previous work by Rufenach (1972) found using amplitude scintillations, that β ranged from 0 to 1 for structure sizes 0.6 to 4 km. Using phase

variations Porcello and Hughes (1968) found β for 2 records

to be 0.8 and 1.0 for auroral conditions.

CHAPTER V

SUMMARY

5.1   Conclusion

A study was made of the inhomogeneous nature of the nocturnal F-region from a ground station at 40.8° N. latitude using phase information from two harmonically related satellite signals. A phase comparison of the two signals eliminated tracking and processing errors common to both, but not the dispersive ionospheric phase modulation. From the phase modulation of the signal, the power spectra of the electron density variations in the diffracting medium (of wavenumber k) was found to follow a power law relationship $P_N'(k) = k^{-(\beta+2)}$. Values of β were found to lie in the range 0.50 to 1.5 with a mean of 0.71 and standard deviation of 0.10. Because of experimental constraints, this expression could only be verified over the range of structure sizes $(2\pi/k)$ from 5.0 to 73 Km.

What is believed to be Fresnel oscillations was also observed in the diffraction pattern. The characteristic nulls in the power spectra of phase variations were present at near the expected frequencies, but due to experimental uncertainties no detailed analysis was performed on them.

Statistical stationarity of the medium w.r.t. the parameter β was considered. Because of the small standard deviation of this value, the exponent $-(\beta + 2)$ appears from the limited sample of ionospheric conditions observed to be

47

a characteristic of the inhomogeneous F-region. One orbital pass did yield a value for β of 1.5, but further measurements would be necessary to examine its significance relative to the above stationarity.

The advantage of the use of phase over amplitude information was made clear by the direct interpretation given here to the data in terms of parameters of the diffracting medium. Amplitude studies have the problem of interpreting the effects of diffraction, as do phase studies for structure sizes below a cutoff value. It is the larger structures which allow observation in the near field and are therefore without major diffraction effects.

5.2   Suggestions for Further Work

This study of the spatial power spectrum of electron density fluctuations in the ionosphere has been constrained in several ways by experimental limitations, and the method could be improved by easing these conditions.

For the smaller scales, less than a few kilometers, diffraction effects complicated the interpretation of data. The use of higher frequencies would extend this range and would also reduce the depth of phase modulation in the ionosphere and thereby lead to a more direct relationship between the diffraction pattern and the medium. However, unless the system noise level could also be reduced for example by the use of higher powers or higher gain (tracking) antennas, and improved recording methods, the extended

range might well be lost in noise due to the lower sensitivity of the effect on higher wave frequencies.

For the large scale end of the spectrum the study has been limited by the finite length of record which can be obtained in the limited field of view of a receiving station. Although some small extension of the range (perhaps a factor of two) might be possible through the use of tracking antennas, this would introduce greater changes in the experimental geometry and further complicate the analysis.

BIBLIOGRAPHY

Appleton, E. V., and M. A. F. Barnett, Local Reflection of Wireless Waves from the Upper Atmosphere, Nature, 115, 333, 1925a.

Blackman, R. B., and J. W. Tukey, The Measurement of Spectra, Dover, 1958.

Briggs, B. H., and I. A. Parkin, On the Variation of Radio Star and Satellite Scintillations with Zenith Angle, J. Atmospheric Terrestrial Phys., 25, 339, 1962.

Cronyn, W. M., The Analysis of Radio Scattering and Space Probe Observation of Small Scale Structure in the Interplanetary Medium, Astrophys. J., 161, 755, 1970.

Dyson, P. L., Direct Measurement of the Size and Amplitude of Irregularities in the Topside Ionsophere, J. Geophysical Res., 74, 6291, 1969.

Elkins, L. J., and M. D. Pagagiannis, Measurement and Interpretation of Power Spectrums of Ionospheric Scintillations at a Sub-Auroral Location, J. Geophysical Res., 74, 4105, 1969.

Herman, J. R., Spread F and Ionospheric F Region Irregularities, Rev. Geophys., 4, 255, 1966.

Jespersen, J. L., G. Kamas, Satellite Scintillation Observation at Boulder, Colorado, J. Atmospheric Terrestrial Phys., 26, 457, 1964.

Jones, I. L., Further Observation of Radio Stellar Scintillations, J. Atmospheric Terrestrial Phys., 19, 26, 1960.

Kelleher, R. F., and J. Sinclair, Some Properties of Ionospheric Irregularities as Deduced from Recordings of the San Marco II and BE-B Satellites, J. Atmospheric Terrestrial Phys., 32, 1259, 1970.

Kuntman, D., A Method for the Determination of Mean Ionospheric Height from Satellite Signals, Scientific Report No. 278, Ionosphere Research Laboratory, The Pennsylvania State University, August 1966.

Lovelace R. V. E., E. E. Salpeter, L. E. Sharp, Analysis of Observations of Interplanetary Scintillation, Astrophys. J., 159, 1047, 1970.

NASA Goddard Space Flight Center, Polar Ionospheric Beacon Satellite (S-66), X-533-63-29, 1963.

Perelygin, V. P., Geomag. Aeron., 9, 281, 1971.

Porcello, L. J., and L. R. Hughes, Observed Fine Structure of a Phase Perterbation Induced during Transauroral Propagation, J. Geophysical Res., 73, 6337, 1968.

Ratcliffe, J. A., Some Aspects of Diffraction Theory and Their Application to the Ionosphere, Reports on Progress in Phys., 19, 188, 1956.

Rastogi, R. G., H. Chandra, M. R. Deshpande, Drift and Anisotropy Parameters of the Irregularities in the E and F Regions of Ionosphere Over Thumba During 1964, J. Atmospheric Terrestrial Phys., 32, 999, 1970.

Rufenach, C. L., Power-Law Wavenumber Spectrum Deduced from Ionospheric Scintillation Observations, J. Geophysical Res., 77, 4761, 1972.

Solomon, S. L. Variations in the Total Electron Content of the Ionosphere at Mid-Latitudes During Direct Sun Conditions, Scientific Report No. 256, Ionosphere Research Laboratory, The Pennsylvania State University, November 1965.

Spencer, M., The Shape of Irregularities in the Upper Atmosphere, Proceeds. Phys. Soc. A, 211, 351, 1955.

E

APPENDIX A

1. The following program was used to take a continuous signal and sample at a uniform rate to produce a data array for digital analysis. The sampling was controlled by a D.C. level on a separate channel of the tape recorder. The comparator (number 34 referenced in lines 170,200 of the program) sensed when the level was + 1 or 0 VDC to control the interrupt subroutines. The comparator was fed into an 'AND' gate along with the clock set at 16 pulses per second. The output was then fed to interrupt 0 (referred to in line 80). The data was fed into the A/D converter channel 0 (referred to in line 230). The data was stored on Dectapes under the file names TEMP1.DAT,TEMP2.DAT etc. in arrays A(4100).

2. The flow diagram in figures 12, 13 is intended as an outline of the method used in data handling and not for use in detailed programming. The following Scientific Subroutine Package programs were used.

Auto: calculates the autocovarience of the data array A

RHARM: calculates the Fourier coefficients of the real data array A.

52

```
              REAL A(4100)
              LOGICAL RSCS
              INTEGER A2(8)
              INTEGER A1(4100)
              EQUIVALENCE (A,A1)
              EXTERNAL ICRAC
              DO 100 I=1,8
              CALL HINIT
              CALL GPI(0,IERR,ICRAC,0,4100,A1)
              CALL STINT
C             START AN ALOG: SET MODE CONTROL TO OP,RUN
              CALL SAMO('OP')
              TYPE 1000
1000          FORMAT('START RECORDER',$)
              ACCEPT 1001,IANS
1001          FORMAT(I)
              CALL SLMO('RUN')
105           IF(RSCS(034)) GO TO 110
              GO TO 105
110           CONTINUE
              IF(RSCS(034)) GO TO 110
              CALL GPISTA(0,.TRUE.,RETURN,4100,INDEX)
              TYPE 500
500           FORMAT('DECTAPE NO. FOR OUTPUT?',$)
              ACCEPT 501,NDT
501           FORMAT(I)
              NDT=NDT+8
              GO TO (1,2,3,4,5,6,7,8),I
1             CALL OFILE(NDT,'TEMP1')
              GO TO 9
2             CALL OFILE(NDT,'TEMP2')
              GO TO 9
3             CALL OFILE(NDT,'TEMP3')
              GO TO 9
4             CALL OFILE(NDT,'TEMP4')
              GO TO 9
5             CALL OFILE(NDT,'TEMP5')
              GO TO 9
6             CALL OFILE(NDT,'TEMP6')
              GO TO 9
7             CALL OFILE(NDT,'TEMP7')
              GO TO 9
8             CALL OFILE(NDT,'TEMP8')
9             WRITE(NDT,10)INDEX,(A1(J),J=1,INDEX)
10            FORMAT(' ',T40,I5/' ',20(1X,I5))
              A2(I)=INDEX
100           CONTINUE
```
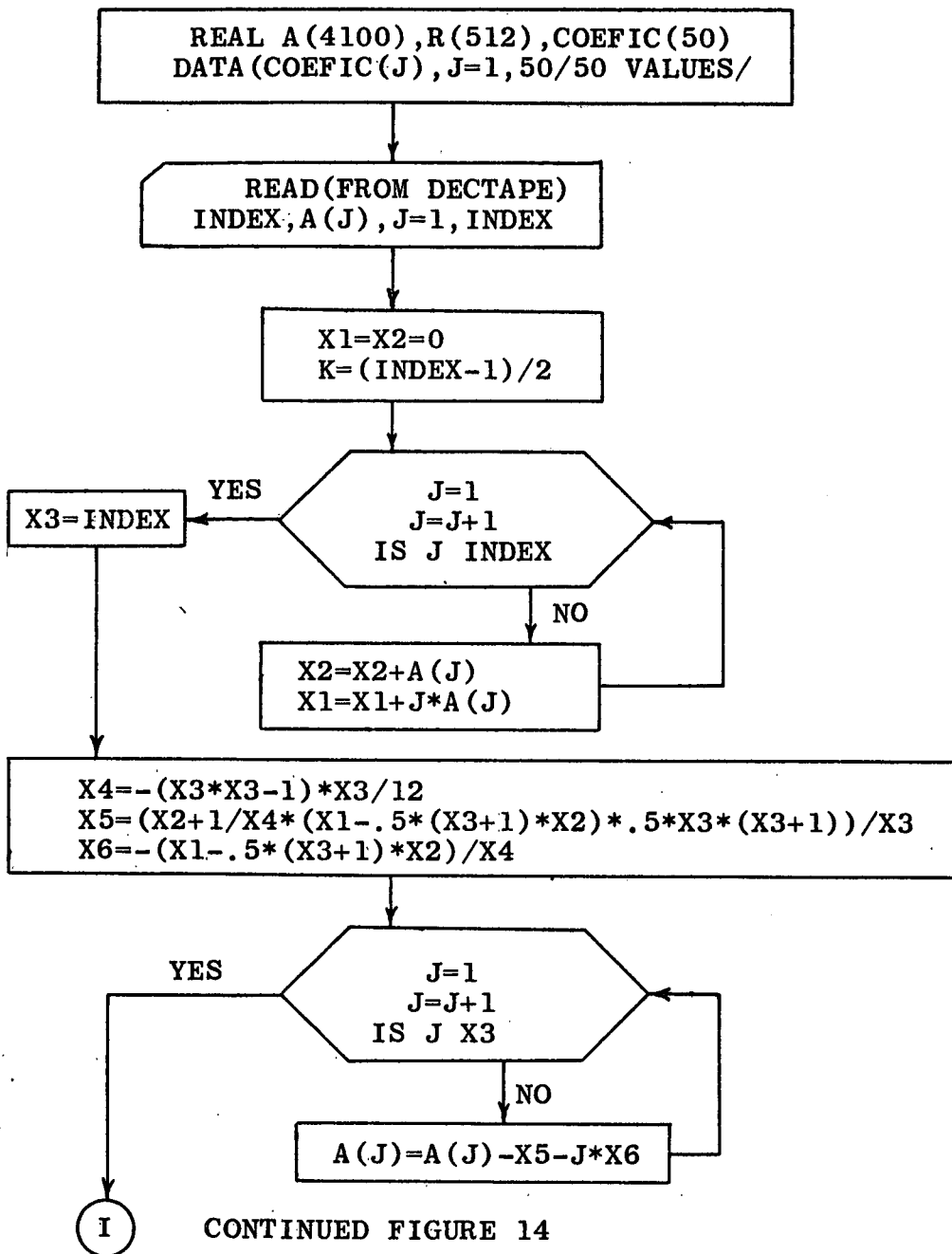
FIGURE 12   FLOW DIAGRAM OF DATA ANALYSIS PROGRAM
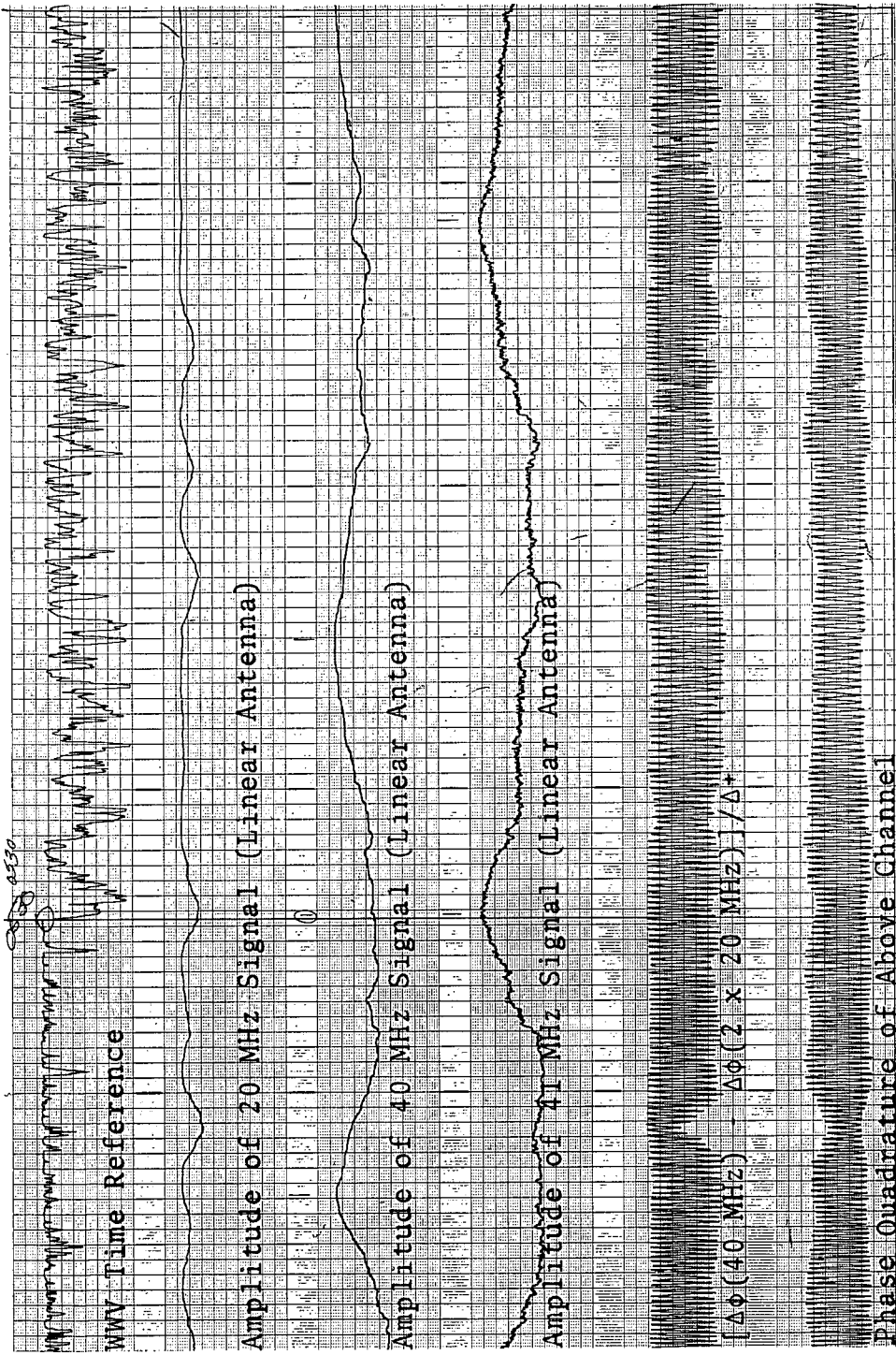
APPENDIX B

Figure 14   Sample of a record of the processed data which
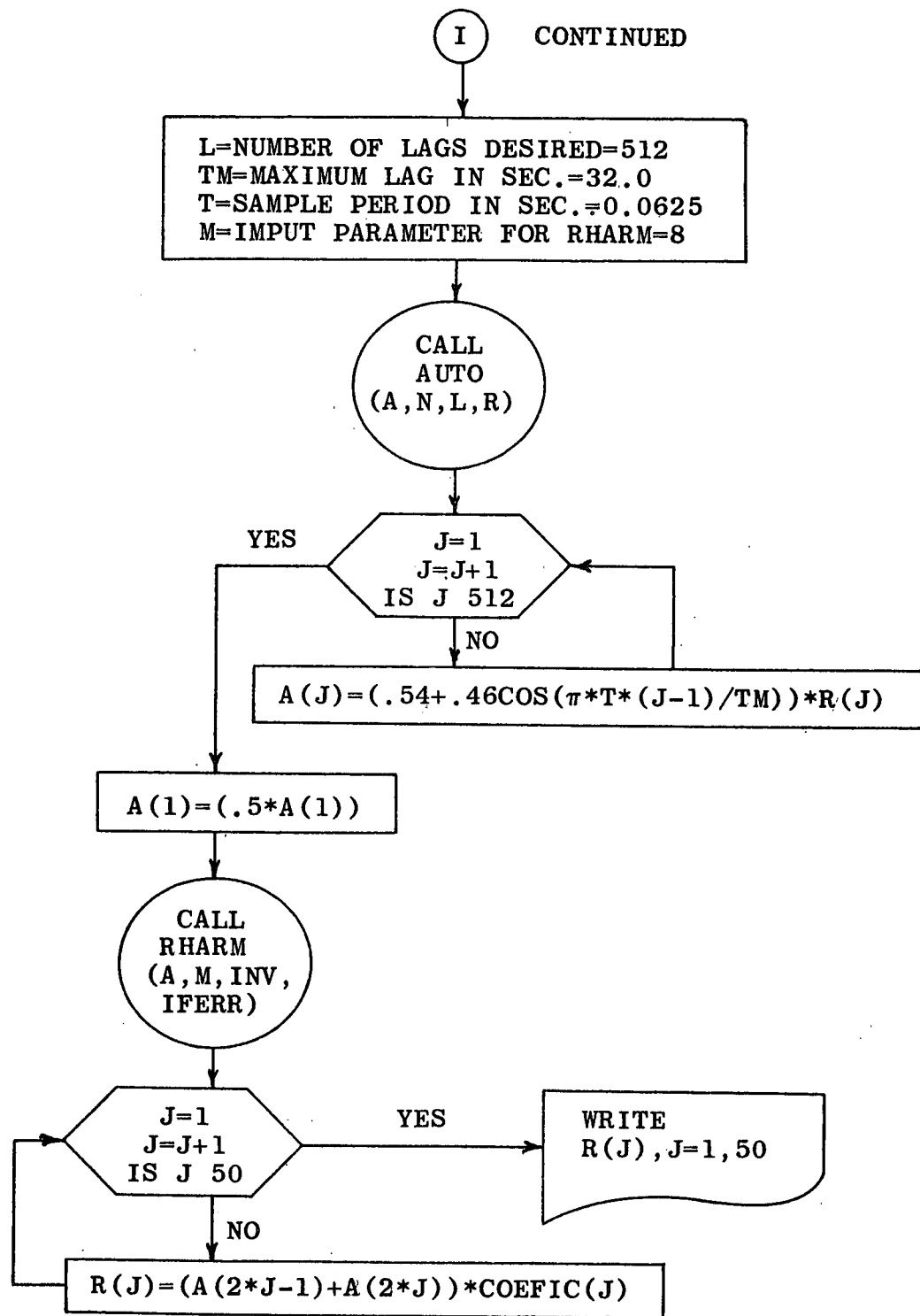is stored before processing on magnetic tape

FIGURE 13 FLOW DIAGRAM (CONTINUED)